Fuel 117 (2014) 1256–1266

Contents lists available at ScienceDirect

Fuel

journal homepage: www.elsevier.com/locate/fuel

Steam gasification of biomass coupled with lime-based CO_2 capture in a dual fluidized bed reactor: A modeling study

Bijan Hejazi [a,*], John R. Grace [a], Xiaotao Bi [a], Andrés Mahecha-Botero [b]

[a] Department of Chemical and Biological Engineering, University of British Columbia, Vancouver, BC V6T 1Z3, Canada
[b] NORAM Engineering, 200 Granville Street, Suite 1800, Vancouver, BC V6C 1S4, Canada

HIGHLIGHTS

- Integrated biomass gasification and cyclic CO_2 capture in a DFB reactor is modeled.
- Limestone particles constitute all or a fraction of the bed material.
- Model predictions are compared against available data from the literature.
- The influence of CO_2 capture on steam gasification of biomass is illustrated.
- Some design and operating conditions could be identified for the gasifier bed.

ARTICLE INFO

Article history:
Received 3 December 2012
Received in revised form 19 July 2013
Accepted 19 July 2013
Available online 8 August 2013

Keywords:
Biomass
Gasification
CO_2 capture
Reactor modeling
CaO sorbent

ABSTRACT

Steam gasification of biomass integrated with CO_2 capture in a dual fluidized bed with carbon sequestration is among the promising technologies being developed for sustainable production of hydrogen. A simple steady state model which considers two coupled reactors, one calcining limestone particles, while the other steam gasifies biomass and simultaneously carbonates the lime sorbent, is developed in this paper. A stoichiometric equilibrium model is applied for biomass gasification, with enhancement of CO_2 removal by carbonation and incomplete conversion of sorbent particles due to kinetic limitations, mixing of the solids and loss of sorbent reactivity because of sintering. To optimize the overall performance of the process, sensitivity analyses are preformed over the most important design and operational parameters. Model predictions are compared with available data from the literature, showing the influence of CO_2 capture on gasification. A parametric study reveals the effects of key process variables such as temperature, pressure and solids circulation rate. The model is useful in identifying design and operating conditions for integrated gasification and carbon capture.

1. Introduction

Emissions of large amounts of Greenhouse Gases (largely CO_2) to the atmosphere, mostly as a by-product of burning fossil fuels in man-made processes, are contributing to climate change. The need to move towards a sustainable energy future is motivating a search for new technologies to address the ever-growing world energy demand. Among the options for reducing greenhouse gas emissions is gasification of biomass. Despite its long history, there is renewed interest in gasification, due to its ability to produce H_2 as a clean energy carrier [1]. Steam gasification of biomass coupled with CO_2 capture, is particularly appealing to produce H_2-rich product gas, with a sorbent to capture CO_2 *in situ* [2]. Enhanced hydrogen production from renewable resources (e.g. biomass) with simultaneous CO_2 capture, when integrated with CO_2 sequestration, could result in net removal of CO_2 from the atmosphere [3]. Lime (CaO) is able to selectively absorb CO_2 through exothermic gas–solid carbonation and reversibly release the captured CO_2 by endothermic calcination:

$$\text{Carbonation}: CaO_{(S)} + CO_2 \leftrightarrow CaCO_{3(S)} \quad \Delta H^0_{298} = -178.2\ \text{kJ/mol} \tag{1}$$

The importance of this reaction lies in its reversibility, facilitating cyclic calcination/carbonation. This process has several advantages including:

I. Enhanced H_2 production due to a shift in the key equilibrium reactions of gasification.
II. Production of a concentrated stream of CO_2, suitable for storage (sequestration).
III. The exothermic carbonation reaction can supply most of the heat demand of the endothermic gasification reactions.
IV. Limestone particles show some catalytic activity for tar cracking and reforming.

* Corresponding author. Tel.: +1 604 827 3178.
E-mail addresses: bhejazi@chbe.ubc.ca, bijanhejazi@gmail.com (B. Hejazi).

0016-2361/$ - see front matter © 2013 Elsevier Ltd. All rights reserved.
http://dx.doi.org/10.1016/j.fuel.2013.07.083

Nomenclature

C_P	isobaric heat capacity, J mol^{-1} K^{-1}
C_{CO2}	actual CO_2 concentration, mol m^{-3}
$C_{CO2,eq}$	equilibrium CO_2 concentration, mol m^{-3}
CCR	CO_2 capture ratio, -
$E(t)$	residence time distribution function, s^{-1}
F_{P1}	molar flow rate of exhaust gas leaving calciner, kmol h^{-1}
F_{P2}	total molar flow rate of product gas leaving carbonator, kmol h^{-1}
F_{air}	molar flow rate of O_2 entering calciner, kmol h^{-1}
h	thickness of $CaCO_3$ product layer, m
H	enthalpy, kJ kmol^{-1}
H^*	stream total enthalpy, kJ kmol^{-1}
HHV	higher heating value, kJ kg^{-1}
k	sorbent deactivation constant, –
K_S	intrinsic kinetic rate constant for carbonation reaction, m^4 mol^{-1} s^{-1}
LHV	lower heating value, kJ kg^{-1} or kJ kmol^{-1}
M	molecular weight, g mol^{-1}
m_{char}	mass flowrate of unreacted char (pure carbon) leaving gasifier, kg h^{-1}
$m_{make\text{-}up}$	mass flowrate of fresh $CaCO_3$ entering calciner (sorbent make-up), kg h^{-1}
m_{purge}	total mass flowrate of $CaCO_3$ and CaO purged from carbonator, kg h^{-1}
m_{PG}	mass flow rate of dry product gas from gasifier, kg h^{-1}
$m_{1,2}$	mass flowrate of CaO cycling from calciner to carbonator, kg h^{-1}
$m_{2,1}$	mass flowrate of $CaCO_3$ and CaO cycling from carbonator to calciner, kg h^{-1}
m_{fuel}	mass flowrate of dry biomass entering carbonator, kg h^{-1}
$m_{mositure}$	mass flowrate of moisture content of biomass entering carbonator, kg h^{-1}
m_{sand}	mass flowrate of circulating silica sand between the two beds, kg h^{-1}
m_{steam}	mass flowrate of steam entering carbonator, kg h^{-1}
$\dot{n}$	stream molar flow rate, kmol h^{-1}
P_0	standard pressure, 1 bar
P_{fuel}	pressure of fuel entering carbonator, kPa
P_{Steam}	pressure of steam entering carbonator, kPa
Q	Net heat source/sink, kJ h^{-1}
Q_{loss}	heat loss, kJ h^{-1}
Q_{in}	external heat stream, kJ h^{-1}
R	universal ideal gas constant, 8.314 J mol^{-1} K^{-1}
S_N	specific surface area available for carbonation in a particle after N cycles, m^2 m^{-3}
S/B	steam to dry biomass ratio, kg kg^{-1}
t	reaction time, s
T_0	standard temperature, 298.15 K
T_1	temperature of reactor 1 (calciner/regenerator), K
T_2	temperature of reactor 2 (carbonator/gasifier), K
T_{fuel}	temperature of fuel entering carbonator, K
T_{Steam}	temperature of steam entering carbonator, K
V_{MCaCO3}	molar volume of $CaCO_3$, m^3 mol^{-1}
w	weight fraction of solid species, –
X_{ave}	overall average carbonation conversion of CaO, –
X_N	maximum conversion of CaO particles at end of fast carbonation stage after Nth cycle, –
$\bar{X}_N$	average carbonation conversion of Nth group of particles, –
$X_N(t)$	conversion of CaO to $CaCO_3$ as function of reaction time and number of cycles,-
X_r	sorbent residual conversion constant, –
y	mole fraction of gaseous species, –

Greek letters

α_N	fraction of sorbent cycled N times, -
η_{CGE}	cold gas efficiency, –
$\Delta H^0_{f,298}$	standard enthalpy of formation of pure substance, kJ kmol^{-1}
λ	stoichiometric oxygen ratio for combustion, –
τ	mean residence time of sorbent particles within carbonator, s
τ_N	time required for particle to reach a conversion of X_N, s
ρ_{CaO}	density of CaO particles, kg m^{-3}

Subscripts

ave	average
carb	carbonator
i	incoming stream and species
ig	ideal gas
j	exit stream
N	cycle number
org	organic species
PG	product gas
solid	inorganic solid species
waf	water- and ash-free

Biomass gasification in the presence of limestone does not date back very far [3–5]. Integrated biomass steam gasification and lime-based CO_2 capture has attracted limited attention, particularly with respect to cyclic operation in a dual fluidized bed reactor configuration [6,7]. Different gasifying agents produce syngas with different calorific values. Steam gasification of biomass produces a medium heating value gas, i.e. 10–18 MJ/Nm^3, attractive compared to N_2-diluted syngas generated from air gasification (4–7 MJ/Nm^3) or the significant power consumption costs and efficiency penalty of an Air Separation Unit required for gasification by O_2-enriched air [8]. Although steam gasification of biofuels is reported to generate more tar in the product gas than air gasification, the higher H_2-content (30–60% vol. dry), originating from partial conversion of H_2O, is attractive [9].

Entrained bed gasifiers are common in fossil fuel gasification, but rarely with biomass feedstock, due to their need for fine material size, high temperature, and economic factors that favor large scale and high pressure operation. Fluidized beds have a long history of solid fuel conversion to useful gaseous products including H_2, CO and light hydrocarbons. Effective heat and mass transfer, temperature uniformity, high solid flow rates and flexibility with regards to the fuel quality are among their advantages relative to entrained and fixed bed gasifiers [3,10].

Dual fluidized beds are particularly important because they can generate a product gas with relatively high concentration of H_2, without product gas dilution by N_2, despite the use of inexpensive air combustion [11], by separating the gasification and combustion in twin vessels. However, improvements are needed to meet commercialization demands, such as the elimination of tars in the product and an increase in steam conversion [1]. Enhancing gasification to produce a cleaner product gas with higher calorific value is a promising alternative [12]. Steam gasification of biomass is a highly endothermic process which takes place at high temperatures (typically > 750 °C). Due to the reversible nature of key gas phase reactions of biomass gasification, the rate of H_2 production is significantly limited by thermodynamic equilibria. Adding a sorbent capable of *in situ* CO_2 capture can shift the equilibrium reactions of biomass gasification (such as reforming and water–gas shift) towards more H_2 formation, while largely satisfying the heat requirements of the endothermic gasification process. In addition, sorbents such as limestone, dolomite, olivine and high-iron solids exhibit some catalytic tar-elimination activity [13].

Despite considerable advancement in both biomass gasification and cyclic lime-based CO_2 capture, these processes have almost always been studied separately. The aim of this paper is to provide a simple, yet useful, model to assist in integrating these two processes. The model allows identification of the most important operational parameters influencing the performance of biomass steam gasification coupled with cyclic CO_2 capture in a dual fluidized bed reactor. It also helps identify some aspects of the process that require further scrutiny.

2. Process description

Fig. 1 shows a schematic of steam gasification of biomass, coupled with *in situ* CO_2 capture. The limestone particles have a dual role: heat carrier and selective transporter of CO_2. Calcined lime (CaO) captures CO_2 under desirable operating conditions of the gasifier/carbonator, producing a H_2-rich product gas through equilibrium shift, while transporting captured CO_2 in the form of $CaCO_3$ to the regenerator/calciner. Within the regenerator, the calcium carbonate particles, accompanied by unreacted char resulting from incomplete carbon conversion, contact pure oxygen. Burning the char particles and additional fuel within the regenerator provides the heat required for sorbent calcination, and thus regenerates lime (CaO) for return to the gasifier. In the present model, complete combustion of unreacted char (carbon) with 10% excess of pure O_2 ($C + O_2 \rightarrow CO_2$) is assumed for the calciner/sorbent regenerator. Based on this simplifying assumption, the purity of CO_2 in the exhaust gas from the calciner exceeds 96% for high sorbent circulation rates. Therefore, the exhaust stream should be of adequate purity for sequestration [14].

Due to the endothermic nature of biomass steam gasification and the heat required for sorbent regeneration in the calciner, direct combustion of unreacted char from the gasifier is usually unable to provide sufficient heat for the process. Indirect heating of the calciner by external heaters or direct burning of char and additional fuel with an oxygen-enriched air stream could provide a high-purity CO_2 stream from the calciner. However, these measures would also increase the concentration of CO_2 within the calciner, thereby promoting sorbent sintering [15,16]. While oxygen-enriched air would reduce the loss of energy by reducing the amount of hot nitrogen leaving the system, the energy required to enrich the air would be much higher than the sensible heat loss with nitrogen. Air combustion of unreacted char and/or additional fuel would lower the calcination temperature at the cost of dilution by nitrogen, unsuitable for sequestration. Lowering the CO_2 partial pressure in the calciner by introducing superheated steam could also lower the calcination temperatures, and satisfy the heat requirement of sorbent regeneration [17]. While steam is a desirable diluent because of its easy subsequent removal from the product CO_2 by condensation, its generation would require extra energy, and it could also affect the structure of the sorbent [18]. Note that in this paper, superheated steam (at 400 °C) is only introduced to the carbonator/gasifier. However, if we intend to introduce steam to the calciner as well, additional heating would be required to increase the temperature of steam to the corresponding regeneration temperature (i.e., >900 °C).

In the present model, we assume a gasifier whose heat demands are mostly met from the sensible heat of bed materials (sand and/or CaO particles) from the regenerator and complete combustion of char from the gasifier, supplemented by an external heat source supplying heat to the regenerator (Q_{in} in Fig. 1). We recognize that complete combustion of carbon with pure O_2 is an oversimplified representation of the actual reactions within the combustor. Several other combustion reactions, together with heterogeneous gasification reactions, determine the final product gas composition and flow rate from the regenerator [19]. Nevertheless, we utilize this simple combustion reaction for the purposes of the model. Under gasification conditions, it is customary to assume instantaneous drying and pyrolysis of solid biomass, resulting in both gaseous products (i.e. H_2, CO, CH_4 and CO_2) and unreacted solid carbon (as char and coke). Assuming perfect mixing of solids in the bubbling bed gasifier (a good assumption [20]), the concentration of unreacted carbon leaving the gasifier is the same as the concentration of solid carbon in the gasifier bed material.

Unreacted carbon from the gasifier originates from two sources [21]: (1) incomplete solid fuel conversion due to thermodynamic limitations, independent of the residence time, but a function of bed temperature, pressure, steam/biomass ratio, etc., and (2) kinetic, mixing and mass transfer limitations. In order to determine the contribution of each of these factors, we need to specify the maximum carbon conversion that is thermodynamically possible

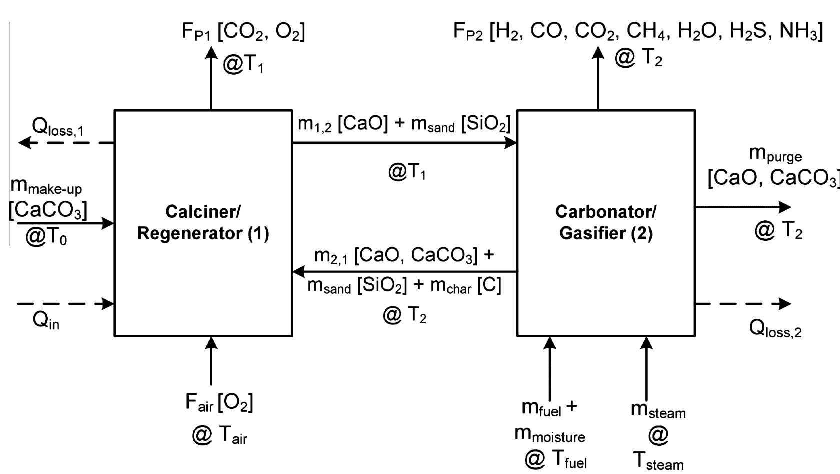

Fig. 1. Schematic of dual vessel system for biomass steam gasification and cyclic CO_2 capture. Dashed and solid arrows are for energy and mass flows, respectively.

within the gasifier (e.g. via the non-stoichiometric model of Li et al. [21]). If operation is outside the coke formation zone, all unconverted carbon (residual char) is due to kinetic reasons (i.e. inadequate residence time). Therefore, the residence time, and hence the circulation rate of bed material, directly influences carbon conversion. Here, for simplification, we lump the overall residual carbon leaving the gasifier into one fraction and assume that it is completely combusted in the regenerator to produce concentrated CO_2 (F_{P1} in Fig. 1). In the presence of non-equilibrium carbonation of calcined limestone, thermodynamic equilibrium is assumed to be achieved for the biomass gasification. The equilibrium modeling approach results in calculations independent of the design of the fluidized bed gasifier [22,23]. However, as the gasifier also operates as a carbonator, a kinetic modeling approach is applied to the carbonation of the sorbent.

3. Model development and simplifying assumptions

In order to develop the model, we assume an equilibrium approach for steam gasification of biomass. Mass and energy balances are expanded to include limestone as well as inert silica sand as part of the bed material (see Fig. 1). A pure $CaCO_3$ sorbent make-up stream is added to the system, and the assumed complete calcination of sorbent particles leads to a stream of pure CaO (together with accompanying sand) circulating from the calciner to the carbonator. Since perfect mixing is assumed, the outlet temperature and composition of the solid and gaseous products are the same as within the respective reactor. The constituents and temperatures of each stream are identified in Fig. 1. Although it is known that thermodynamic equilibrium may not be fully achieved because of the relatively low operation temperatures, models based on thermodynamic equilibrium are used widely with reasonable success [21–23]. In this paper, to predict the highest gasification or thermal efficiency that could be attained within the gasifier for a given feedstock, the product gas composition is assumed to be governed by equilibrium calculations. We consider CH_4, CO, CO_2, H_2, and H_2O as the main components coming to thermodynamic equilibrium in the presence of solid carbon C. As a simplifying assumption and due to their low contents in the fuel, sulfur and nitrogen are assumed to be completely converted to hydrogen sulfide (H_2S) and ammonia (NH_3), respectively [23,24]. Future work should take into account what other N and S compounds are formed. Furthermore, the formation of tars, any catalytic effect (but not the sorbent effect) of limestone on the composition of the product stream, and the ash content of the fuel are neglected, and solid biomass is described by its ultimate analysis.

The gasifier product gas composition is predicted by implementing an overall mass balance for each main element (C,H,O,N,S) over the gasification zone, together with equations for the chemical equilibrium of three independent reactions (Boudouard, methanation and heterogeneous water–gas reactions). Note that these three heterogeneous reactions can be reduced to two when no solid carbon remains at equilibrium. Therefore, the following equilibrium relations describe the biomass gasification [23]:

(i) With solid carbon:

$$C_{(S)} + CO_2 \leftrightarrow 2CO \quad \Delta H^0_{298} = 172.5\ \text{kJ/mol} \tag{2.a}$$

$$C_{(S)} + 2H_2 \leftrightarrow CH_4 \quad \Delta H^0_{298} = -73\ \text{kJ/mol} \tag{2.b}$$

$$C_{(S)} + H_2O \leftrightarrow CO + H_2 \quad \Delta H^0_{298} = 131.3\ \text{kJ/mol} \tag{2.c}$$

(ii) Without solid carbon:

$$CO + H_2O \leftrightarrow CO_2 + H_2 \quad \Delta H^0_{298} = -41.2\ \text{kJ/mol} \tag{3.a}$$

$$CH_4 + H_2O \leftrightarrow CO + 3H_2 \quad \Delta H^0_{298} = 206\ \text{kJ/mol} \tag{3.b}$$

Although the influence of the unreacted char/fuel ratio on the thermal efficiency of the process is obvious, for the conditions of interest of this study it is assumed that no solid carbon remains at equilibrium. Therefore, the residual carbon leaving the gasifier originates solely from kinetic limitations. Hence, it is set at a typical 15 wt% of the carbon content of the fuel [23].

Starting with elemental mass balances over the complete system, indicated in Fig. 1, and constrained by the above equilibrium gas-phase reactions, we must also account for the enhancement effect of lime. This is achieved by extending the elemental mass balances to account for Ca-containing compounds (i.e. CaO, $CaCO_3$), while also performing Ca balances over both reactors. To specify the CO_2 capture from the gasification zone, we also need to find the degree of carbonation of CaO particles within the gasifier/carbonator as discussed in the next section. The simulation algorithm is summarized in Fig. 2. The resulting system of non-linear algebraic equations is solved using MATLAB software. This system consists of six elemental mass balances (C and Ca for the calciner and C, H, O and Ca for the carbonator), coupled with two equilibrium equations (Eqs. (3.a) and (3.b)) representing biomass gasification. Energy balances are preformed over both reactors to find the external heat requirement of the process (Q_{in}), circulation rate of bed material between the two reactors and the limestone fraction of the carbonator bed. Table 1 includes the mass and energy balance calculations corresponding to the streams in Fig. 1.

The energy balance calculations use a general methodology [25]. Regardless of the reactions considered, it is only based on mixture thermodynamic enthalpies of all inlet and outlet streams crossing the system boundaries. In this manner, the thermodynamic states of streams and the heats of reaction are taken into account implicitly. We have:

$$Q = \sum_j \dot{n}_j \cdot H^*_j(P_j, T_j) - \sum_i \dot{n}_i \cdot H^*_i(P_i, T_i) \tag{4}$$

where Q is the net incoming heat (positive for heat sources), $\dot{n}_i$ and $H^*_i(P_iT_i)$ are the molar flow rate and total enthalpy of incoming streams at their respective temperatures and pressures, while $\dot{n}_j$ and $H^*_j(P_jT_j)$ are the molar flow rate and total enthalpy of exiting streams, respectively.

To describe the thermodynamic states of the streams involved, substances are divided into four classes, i.e. ideal gases, inorganic solids, organic substances and pure water/steam [25]. NASA-polynomials are used to calculate isobaric heat capacities of ideal gases and inorganic solid species [26]. The empirical correlations of Boie, as adopted in [25], and Merrick [27] are applied to calculate the lower heating value of dry and ash-free biomass (LHV_{fuel}) and the enthalpy and heat capacity of char as a function of temperature, respectively. IAPWS-IF97 [28,29] is used to estimate the enthalpy of sub-cooled liquid water (i.e. biomass moisture content) and superheated steam.

3.1. Finding the average carbonation conversion

The effectiveness of limestone particles decays due to:

- Pore blockage by $CaSO_4$ originating from the sulfur content of the biomass.
- Attrition, leading to mechanical fragmentation and entrainment from the system.
- Loss of specific area due to sintering.

Deactivation of sorbent particles due to coke formation covering active CaO sites could also compete significantly with the carbonation reaction and hamper effective CO_2 capture

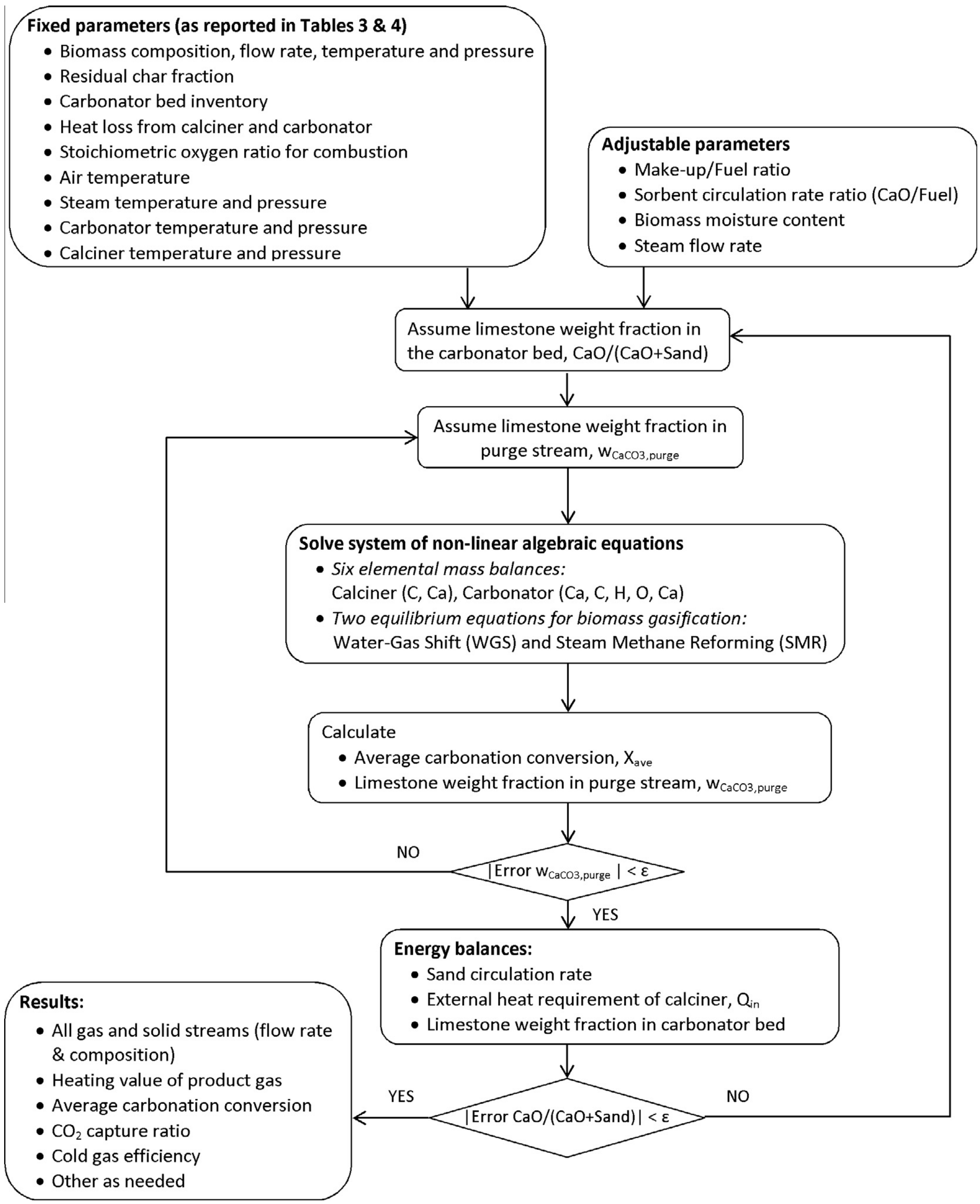

Fig. 2. Algorithm of simulation.

[9,30]. For the current model, the effects of attrition, entrainment, coke formation and pore blockage by $CaSO_4$ are neglected, but loss of reactivity due to sintering is taken into account. Sintering, the main contributor to decreasing CO_2 carrying capacity of the sorbent, occurs mostly during calcination [31]. SEM images demonstrate sorbent particles going through multiple capture and release cycles, decreasing in micro-porosity and increasing in meso-porosity, leading to loss of surface area available for CO_2 capture [32]. In addition, previous research shows that a fast, chemically controlled, initial carbonation stage is followed by a second slower reaction stage controlled by diffusion through the $CaCO_3$ layer [33–35]. Transition between the fast and slow stages takes place quite abruptly. The maximum achievable degree of carbonation of sorbent particles at the end of the fast carbonation period decreases with each cycle at the same temperature and the same carbonation time. This limiting conversion determines the overall reactor performance with gas–solid contact sufficient to ensure that most sorbent particles complete the fast reaction stage [34]. To maintain steady-state operation of the system and keep the average carbonation conversion constant, it is essential to compensate for the reactivity loss of the sorbent by replacing some "old" particles with fresh sorbent particles. To find the maximum achievable average carbonation conversion of a CaO population over N carbonation-calcination cycles, we write:

$$X_{ave} = \sum_{N=1}^{\infty} \alpha_N \cdot X_N \tag{5}$$

where X_N is the maximum utilization efficiency of CaO particles at the end of the fast carbonation period after the Nth cycle and α_N is the

Table 1
Mass and energy balance calculations corresponding to Fig. 1.

Mass balances:

<u>Carbonator</u> :

$$C : \frac{m_{fuel} w_C}{C} - \frac{(m_{purge} + m_{2,1}) w_{CaCO_3}}{MW_{CaCO_3}} - \frac{m_{char}}{C} - F_{P2}(y_{CO_2} + y_{CO} + y_{CH_4}) = 0$$

$$H : \frac{m_{fuel} w_H}{H} + \frac{2 \times (m_{moisture} + m_{steam})}{MW_{H_2O}} - F_{P2}(2 \times y_{H_2} + 4 \times y_{CH_4} + 2 \times (1 - (y_{H_2} + y_{CH_4} + y_{CO} + y_{CO_2}))) = 0$$

$$O : \frac{m_{fuel} w_O}{O} + \frac{(m_{moisture} + m_{steam})}{MW_{H_2O}} + \frac{m_{1,2}}{MW_{CaO}} - (m_{purge} + m_{2,1})\left(\frac{3 \times w_{CaCO_3}}{MW_{CaCO_3}} + \frac{1 - w_{CaCO_3}}{MW_{CaO}}\right)$$
$$- F_{P2}(y_{CO} + 2 \times y_{CO_2} + (1 - (y_{H_2} + y_{CH_4} + y_{CO} + y_{CO_2}))) = 0$$

$$Ca : \frac{m_{1,2}}{MW_{CaO}} - (m_{purge} + m_{2,1})\left(\frac{w_{CaCO_3}}{MW_{CaCO_3}} + \frac{1 - w_{CaCO_3}}{MW_{CaO}}\right) = 0$$

<u>Calciner</u> :

$$C : \frac{m_{makeup}}{MW_{CaCO_3}} + \frac{m_{2,1} \cdot w_{CaCO_3}}{MW_{CaCO_3}} + \frac{m_{char}}{C} - F_{P1} \cdot y_{CO_2,P1} = 0$$

$$Ca : \frac{m_{makeup}}{MW_{CaCO_3}} + m_{2,1}\left(\frac{w_{CaCO_3}}{MW_{CaCO_3}} + \frac{1 - w_{CaCO_3}}{MW_{CaO}}\right) - \frac{m_{1,2}}{MW_{CaO}} = 0$$

Note assumptions : Char is assumed to be pure carbon. H_2S and NH_3 are neglected. SiO_2 is not considered in oxygen balances.

Equilibrium equations:

$$\text{WGS} : 10^{(2048/T^{-1.896})} - \frac{y_{CO_2} \times y_{H_2}}{y_{CO} \times (1 - (y_{CO_2} + y_{CO} + y_{CH_4} + y_{H_2}))} = 0$$

$$\text{SMR} : 10^{(-11{,}238/T^{+12.62})} - \frac{y_{CO} \times y_{H_2}^3}{y_{CH_4} \times (1 - (y_{CO_2} + y_{CO} + y_{CH_4} + y_{H_2}))} \times \left(\frac{P}{P_0}\right)^2 = 0$$

Energy balances:

<u>Carbonator</u> :

$$m_{fuel} \cdot H^*_{fuel}(T_{fuel}) + m_{moisture} \cdot H^*_{H_2O}(T_{fuel}, P_{fuel}) + m_{steam} \cdot H^*_{steam}(T_{steam}, P_{steam}) + m_{1,2} \times H^*_{CaO}(T_1) + m_{sand} \cdot H^*_{SiO_2}(T_1)$$
$$- m_{sand} \cdot H^*_{SiO_2}(T_2) - m_{char} \cdot H^*_{char}(T_2) - (m_{purge} + m_{2,1}) \times (w_{CaCO_3} \cdot H^*_{CaCO_3}(T_2) + (1 - w_{CaCO_3}) \cdot H^*_{CaO}(T_2)) - Q_{loss,2}$$
$$- F_{p2} \cdot \left(\textstyle\sum_{ii \neq H_2O} y_i \cdot H^*_i(T_2) + y_{H_2O} \cdot H^*_{H_2O}(T_2, P_2)\right) = 0$$

<u>Calciner</u> : $Q_{in} + F_{air} \cdot H^*_{O_2}(T_{air}) + m_{makeup} \cdot H^*_{CaCO_3}(T_0) + m_{char} \cdot H^*_{char}(T_2) + m_{2,1} \times (w_{CaCO_3} \cdot H^*_{CaCO_3}(T_2) + (1 - w_{CaCO_3}) \cdot H^*_{CaO}(T_2))$

$$+ m_{sand} \cdot H^*_{SiO_2}(T_2) - F_{CO_2,P1} \cdot H^*_{CO_2}(T_1) - F_{O_2,P1} \cdot H^*_{O_2}(T_1) - m_{1,2} \times H^*_{CaO}(T_1) - m_{sand} \cdot H^*_{SiO_2}(T_1) - Q_{loss,1} = 0$$

<u>Overall</u> : $Q_{in} + F_{air} \cdot H^*_{O_2}(T_{air}) + m_{fuel} \cdot H^*_{fuel}(T_{fuel}) + m_{moisture} \cdot H^*_{H_2O}(T_{fuel}, P_{fuel}) + m_{steam} \cdot H^*_{steam}(T_{steam}, P_{steam})$

$$+ m_{makeup} \cdot H^*_{CaCO_3}(T_0) - m_{purge} \times (w_{CaCO_3} \cdot H^*_{CaCO_3}(T_2) + (1 - w_{CaCO_3}) \cdot H^*_{CaO}(T_2)) - F_{CO_2,p1} \cdot H^*_{CO_2}(T_1) - F_{O_2,p1} \cdot H^*_{O_2}(T_1)$$
$$- Q_{loss,1} - Q_{loss,2} - F_{p2} \cdot \left(\textstyle\sum_{ii \neq H_2O} y_i \cdot H^*_i(T_2) + y_{H_2O} \cdot H^*_{H_2O}(T_2, P_2)\right) = 0$$

Assumption: Negligible sand mass flowrate in purge stream.

fraction of sorbent particles that have experienced N sorption–desorption cycles. It is customary to express X_N as a function of the cycle number [34,35]. Grasa and Abanades [34] fitted experimental results up to 500 cycles and a wide range of operating conditions by

$$X_N = \frac{1}{1/(1 - X_r) + kN} + X_r \tag{6}$$

where k and X_r are a fitted deactivation constant and the residual conversion, respectively, both depending on the sorbent characteristics. Typical values of $k = 0.52$ and $X_r = 0.075$ obtained by Grasa and Abanades [34] are used in this study. These values could be modified if the negative effect of sulfation is taken into account [36]. Note that Eq. (6) only considers the fast (kinetically-controlled) stage of carbonation where solid conversion under the diffusion controlled regime is not yet important. This approach is limited to carbonation times less than about 5 min, carbonation temperature of about 650 °C and average CO_2 partial pressures less than 0.1 bar [37].

During steady-state operation, particles of different ages are continuously fed to the carbonator. The proportion of these particles ranges from α_1 (for particles freshly introduced to the system from the make-up stream) to α_∞ (for particles not yet purged which have remained in the system for many cycles). To determine the population distribution of these particles, the fraction of particles entering the carbonator that have circulated N times, α_N, is calculated from a succession of mole balances over Ca [38]:

$$\begin{aligned} \alpha_1 &= \frac{\text{Ca introduced from make-up stream}}{\text{Total Ca in the stream entering the carbonate}} \\ \alpha_2 &= \alpha_1(1 - \alpha_1) \\ &\vdots \\ \alpha_N &= \alpha_1(1 - \alpha_1)^{N-1} \end{aligned} \tag{7}$$

Substituting Eqs. (6) and (7) into Eq. (5) gives

$$X_{ave} = \sum_{N=1}^{\infty} \alpha_1(1 - \alpha_1)^{N-1} \cdot \left(\frac{1}{1/(1 - X_r) + kN} + X_r\right) \tag{8}$$

As discussed by Rodriguez et al. [39] and Grasa et al. [40], the fraction of particles which have experienced a number of complete carbonation–calcination cycles (reaction age, N_{age}) can be expressed as a function of the actual carbonation and calcination levels in each reactor. Therefore, when computing the capture capacity of a sorbent particle, the equivalent number of complete carbonation–calcination cycles (N_{age}) should be considered rather than the number of passages (N) between the two reactors. As our main objective is to develop a relatively simple model that captures the essence of integrated biomass gasification with cyclic CO_2 capture in a dual fluidized bed reactor, reaction age is not considered in this paper.

By averaging over the reactivity of different groups of particles entering the carbonator from $N = 1$ (freshly added) to $N = \infty$ (aged to their residual reactivity), we account for the loss of sorbent reactivity during cyclic operation due to sintering. While it is reasonable to assume that the calciner is sufficiently large, or the calcination rate fast enough, to allow all particles to convert fully from $CaCO_3$ to CaO within the calciner, several issues remain to be addressed for the carbonator. Owing to factors other than sintering, such as non-uniform residence time distribution and chemical kinetic limitations, sorbent particles do not carbonate completely within the reactor. In most fluidized bed reactors, the mean residence time of particles is much larger than their turnover time, and perfect mixing of solid particles is then a reasonable approximation. Because of the distribution of residence times for particles entering the carbonator, CaO particles have unequal chances of being carbonated. Previous studies [40,41] demonstrate that during carbonation, a $CaCO_3$ product layer forms on the outer surface of particles, causing resistance to further CO_2 diffusion to the unreacted CaO core. To account for the mixing and the kinetic limitation of the carbonation reaction, we consider the Residence

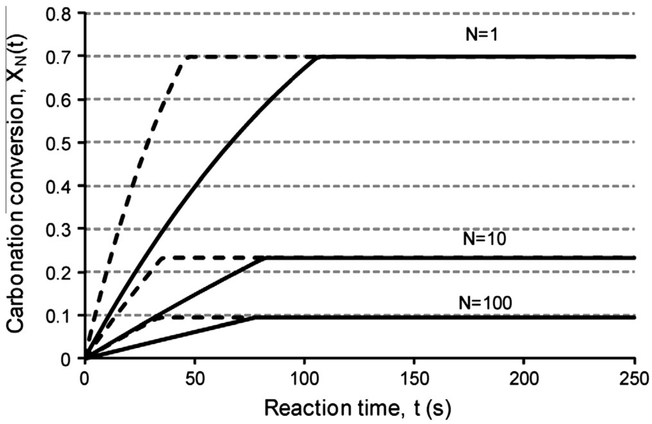

Fig. 3. Sorbent conversion versus time for particles subjected to different number of carbonation cycles (Dashed lines: P_{CO2} = 10 kPa; solid lines: P_{CO2} = 5 kPa) at atmospheric pressure. Carbonation temperature 650 °C (adapted from Romano [45]).

Table 2
Parameters used to calculate sorbent conversion [45].

K_S (m^4/mol/s)	V_{MCaCO3} (m^3/mol)	ρ_{CaO} (kg/m^3)	h (m)	k (–)	X_r (–)
6.05×10^{-10}	36.9×10^{-6}	3320	50×10^{-9}	0.52	0.075

Time Distribution (RTD) of solid material in the carbonator, combined with a suitable model for the carbonation rate of CaO particles as a function of cycle number (N). With the assumptions of uniform CO_2 concentration and perfect mixing of sorbent particles, the conversion of CaO in individual particles depends on their duration within the reactor. Different particles, despite belonging to the same cycle number, experience different reaction times within the carbonator. Hence, in addition to our earlier classification of entering particles to the carbonator based on the number of cycles previously experienced (α_N in Eq. (5)), we also need to account for their distribution of residence times within the carbonator. For a mean residence time of τ, the perfect mixing RTD function is:

$$E(t) = \exp(-t/\tau)/\tau \tag{9}$$

The representative average carbonation conversion of the Nth group of particles is approximated by:

$$\bar{X}_N = \int_0^\infty X_N(t) \cdot E(t)dt \tag{10}$$

Here $X_N(t)$ is the conversion of CaO to $CaCO_3$ both as a function of reaction time and number of cycles (N) experienced by CaO particles. To find the overall average carbonation conversion for all CaO particles, we need to replace X_N from Eq. (5) (in which only the effect of sorbent sintering is taken into account) by:

$$X_{ave} = \sum_{N=1}^{\infty} \alpha_N \cdot \bar{X}_N \tag{11}$$

Substituting Eq. (10) into Eq. (11), the overall average carbonation conversion is then

$$X_{ave} = \sum_{N=1}^{\infty} \alpha_N \cdot \left(\int_0^\infty X_N(t) \cdot E(t)dt \right) \tag{12}$$

Various approaches have been suggested to simulate the carbonation rate of limestone particles, ranging from simple homogeneous grain models to the Shrinking Core and Pore models. However, most of these expressions require several fitted parameters that limit their applicability to a specific set of experimental conditions and/or a specific sorbent. Grasa et al. [42] suggested that a simple first order kinetic model is sufficient to describe the carbonation of highly cycled particles during the fast reaction phase usually encountered in industrial applications. Although they neglected the effects of intra-particle and transport resistances, the wide range of reaction conditions, particle sizes and sorbents used to find the curve-fitting parameters give credibility to their approach. The first-order carbonation rate expression is then:

$$dX_N(t)/dt = K_S S_N (1 - X_N(t))^{\frac{2}{3}} (C_{CO2} - C_{CO2,eq}) \tag{13}$$

where K_S is an intrinsic kinetic constant, S_N the specific surface area available for reaction in a particle which has experienced N carbonation-calcination cycles, and C_{CO2} and $C_{CO2,eq}$ are the actual and equilibrium CO_2 concentrations. With the dependence of the equilibrium partial pressure of CO_2 on the decomposition temperature of $CaCO_3$ based on a semi-empirical correlation proposed by Baker [43] and ideal gas law behavior, $C_{CO2,eq}$ is given as a function of carbonation temperature:

$$C_{CO2,eq}(\mathrm{mol/m^3}) = 10^{(-8308/T)+9.079}(\mathrm{kPa})/RT \tag{14}$$

From Eq. (13), the dependence of the carbonation rate of particles on the cycle number is seen through particle available surface area, which in turn is proportional to the maximum carbonation degree at the end of the fast carbonation period (X_N):

$$S_N = \rho_{CaO}(V_{MCaCO_3} X_N / M_{CaO} h) \tag{15}$$

Here V_{MCaCO3} is the molar volume of $CaCO_3$, M_{CaO} and ρ_{CaO} are the molecular mass and density of CaO, respectively, and h is the thickness of the $CaCO_3$ product layer, found to be about 50 nm and almost constant during cycling [44].

Upon integration of Eq. (13), the carbonation degree of a CaO-based particle can be expressed explicitly by:

$$X_N(t) = 1 - (1 - (K_S S_N (C_{CO2} - C_{CO2,eq}/3)t))^3 \quad \text{for } t \leqslant \tau_N \tag{16}$$

where τ_N is the time required for a particle to reach a conversion of X_N:

$$\tau_N = 3(1 - (1 - X_N)^{1/3})/K_S S_N (C_{CO2} - C_{CO2,eq}) \tag{17}$$

As noted above, sintering imposes an upper limit on the maximum achievable conversion of particles that have experienced N calcination-carbonation cycles at a given temperature and time of carbonation. Hence, for $t > \tau_N$, $X_N(t)$ remains constant. The conversion of sorbent particles is plotted versus time in Fig. 3, for different cycle numbers and CO_2 concentrations, with the parameters reported in Table 2 [45].

Overall, Eq. (12) can be rewritten to find the overall average carbonation conversion:

$$X_{ave} = \sum_{N=1}^{\infty} \alpha_N \cdot \left(\int_0^{\tau N} X_N(t) \cdot E(t)dt + X_N \int_{\tau N}^{\infty} E(t)dt \right) \tag{18}$$

From Eq. (18), the average carbonation conversion of CaO particles within the carbonator is related not only to the carbonator operating conditions (e.g. temperature, CO_2 partial pressure and mean residence time of sorbent particles), but also restricted by the degree of sintering during cyclic operation.

4. Results and discussion

The effects of different process parameters such as biomass moisture content, steam-to-biomass ratio (S/B), sorbent make-up to dry fuel ratio (M/F), sorbent circulation rate ratio, carbonator

Table 3
Average properties of six sawdust species [21].

Proximate analysis and other properties		Ultimate analysis (wt%, dry and ash-free)	
HHV (MJ/kg)	20.6	C	51.5
Moisture content	15	H	6.7
Ash content (wt%)	1.14	O	41.0
Dry bulk density (kg/m^3)	220	N	0.52
Mean particle diameter (mm)	0.79	S	0.34

Table 4
Process parameters for all simulations.

Dry biomass flow rate	100 kg/h
m^*_{fuel} LHV_{fuel}	551.4 kW
Residual char fraction	15 wt% Fuel carbon content
Gasifier bed inventory	75 kg
$Q_{loss,combustor} = Q_{loss,gasifier}$	2.5% (m^*_{fuel} LHV_{fuel})
λ (molar ratio)= O_2/C	1.1
T_{air}	300 °C
T_{steam} and P_{steam}	400 °C and 1 atm
T_{fuel} and P_{fuel}	25 °C and 1 atm

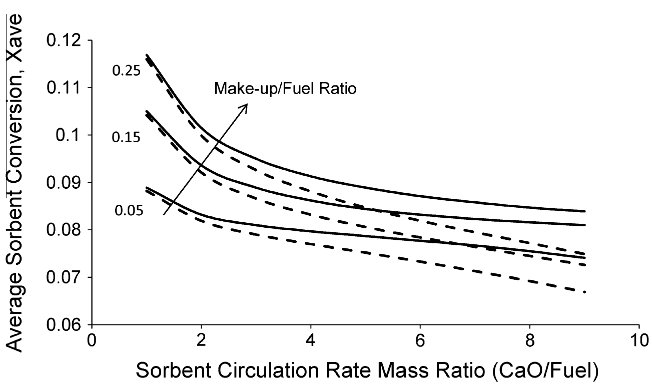

Fig. 4. Average sorbent carbonation conversion as a function of make-up/fuel ratio and sorbent circulation rate ratio. Dashed and solid curves are for realistic (Eq. (18)) and maximum (Eq. (8)) carbonation conversions, respectively. T_{Carb} = 650 °C, P_{Carb} = 1 atm, Steam/Biomass = 0.7, Biomass moisture content = 15 wt%.

bed inventory of sorbent, gasification temperature (T_2) and pressure (P_2) were first studied through sensitivity analyses. Metrics are defined as:

$$\text{Biomass moisture content} = m_{moisture}/(m_{moisture} + m_{fuel}) \tag{19}$$

$$\text{Steam/Biomass ratio}(S/B) = (m_{moisture} + m_{steam})/m_{fuel} \tag{20}$$

$$\text{Sorbent make-up/fuel ratio} = M_{make\text{-}up}[CaCO_3]/m_{fuel} \tag{21}$$

$$\text{Sorbent circulation rate ratio} = m_{1,2}[CaO]/m_{fuel} \tag{22}$$

$$\text{Carbonation conversion}(X_{ave}) = \frac{\text{CaO converted to}CaCO_3\text{within the carbonator}}{\text{Total CaO entering the carbonator}} \tag{23}$$

where m_{fuel} and $m_{moisture}$ are the mass flowrates of dry biomass and moisture content of biomass entering carbonator, m_{steam} is the mass flowrate of fluidizing steam, $m_{make\text{-}up}$ the mass flowrate of fresh $CaCO_3$ entering the calciner, and $m_{1,2}$ the mass flowrate of CaO cycling from calciner to carbonator.

The effective molar abundances of dry ash-free biomass ($CH_{1.5568}O_{0.5968}N_{0.0087}S_{0.0025}$) are based on the average ultimate analyses of six woody biomass species investigated by Li et al. [21,24], as summarized in Table 3. Constant process parameters for the simulations are given in Table 4.

Fig. 4 illustrates the average predicted carbonation conversion of CaO particles within the gasifier as a function of make-up/dry fuel ratio and sorbent circulation rate ratio, with solid and dashed curves corresponding to Eqs. (8) and (18), respectively. While X_{ave} increases with increasing make-up/fuel ratio, it is predicted to decrease monotonically with increasing sorbent circulation rate ratio. This occurs because introducing more fresh sorbent particles from the make-up stream increases the number of particles that have experienced fewer cycles (suffering less sintering). In the case of the kinetically-modified model (dashed curves), due to the strong dependency of X_{ave} on the mean residence time of sorbent particles within the carbonator, lower average carbonation conversions are observed at higher circulation rates.

For lime-enhanced steam biomass gasification, it is also of interest to see how the CO_2 capture ratio, CCR, defined as the ratio of the CO_2 captured by the lime to all carbon converted to CO_2 within the gasifier, is affected by the operating conditions. As shown in Fig. 5, CCR increases with increasing make-up/fuel ratio and increasing sorbent/fuel ratio due to increased CaO surface area available for CO_2 capture. As with the average carbonation conversion, the effect of decreased residence time at higher circulation rates is more significant in decreasing the CO_2 capture ratio. At higher circulation rates, lower carbonation conversion reduces the $CaCO_3$ weight fraction in the purge stream from the carbonator, while higher CO_2 capture efficiencies lead to higher CO_2 flow rates from the calciner. These results are consistent with experimental and modeling results [45,46]. However, the predicted CCR is lower than reported in the literature, mainly because of lower CO_2 partial pressures resulting from homogeneous gasification reactions as opposed to capture from pure CO_2. The parameter values used in this study (Table 2), calculated for repeatedly cycled particles [45], may also contribute to the discrepancy. The values of other adjustable parameters are summarized in the captions of Figs. 4 and 5. Our remaining predictions are based on Eq. (18).

Optimizing the solid circulation rate between the beds is of paramount importance for effective CO_2 capture and heat delivery. The effect of circulation rate ratio on both dry product gas composition (wet basis for H_2O) and flow rate from the gasifier is shown in Fig. 6. With increasing sorbent circulation rate, the CO_2 concentration within the carbonator decreases (dashed curve), shifting the water–gas shift reaction towards more H_2 production and CO consumption. The small increase in CH_4 equilibrium concentration is due to methanation (reverse of steam methane reforming) at high H_2 concentrations. In total, due to the higher carbon capture and production of a product gas richer in H_2 at higher sorbent

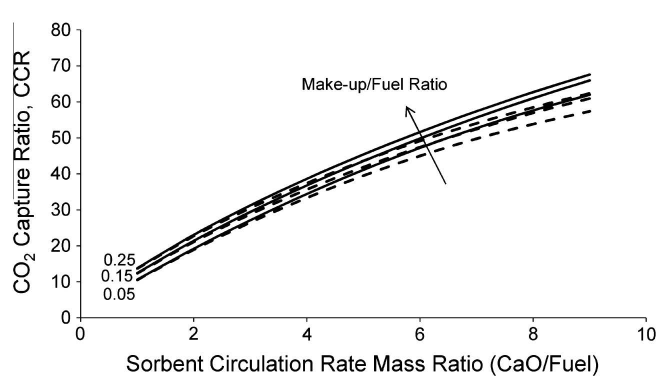

Fig. 5. CO_2 capture ratio as a function of make-up/fuel ratio and sorbent circulation rate ratio. Dashed and solid curves are for realistic (Eq. (18)) and maximum (Eq. (8)) carbonation conversion respectively. T_{Carb} = 650 °C, P_{Carb} = 1 atm, Steam/Biomass = 0.7, Biomass moisture content = 15 wt%.

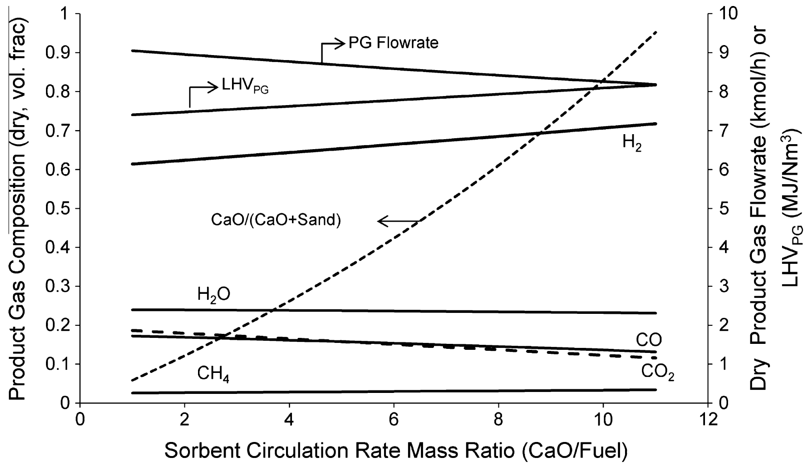

Fig. 6. Effect of sorbent circulation rate ratio on dry product gas composition and flow rate from carbonator/gasifier. Dotted curve is for limestone weight fraction of bed material. T_{carb} = 650 °C, P_{carb} = 1 atm, Steam/Biomass = 0.7, biomass moisture content = 15 wt%, sorbent makeup/fuel = 0.1.

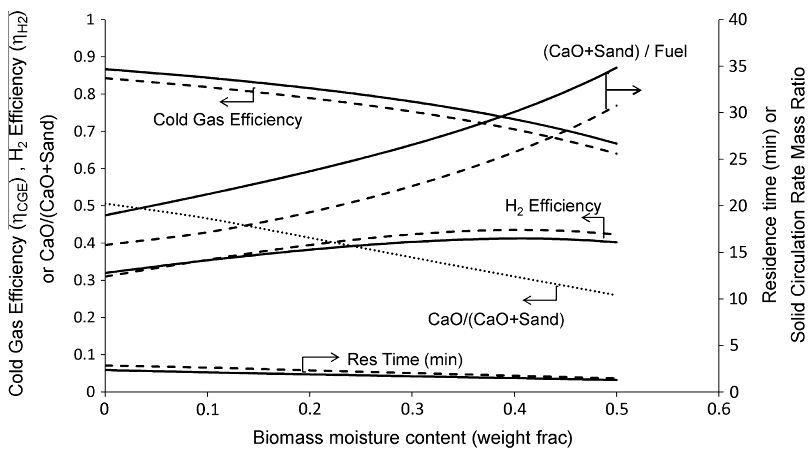

Fig. 7. Comparison of lime-enhanced and non-enhanced biomass gasification cold gas efficiency, H_2 efficiency, limestone weight fraction of bed material, and solids residence time within carbonator. Solid and dashed curves are for non-enhanced and lime-enhanced biomass gasification, respectively. Dotted curve is for limestone weight fraction of bed material. T_{carb} = 700 °C, T_{calc} = 925 °C, P_{carb} = 1 atm, CaO/Fuel = 8, sorbent makeup/fuel = 0.1 (constant steam flow rate).

circulation rates, the Lower Heating Value of the dry product gas from the gasifier increases, while its total flow rate decreases. For these operating conditions, the partial pressure of CO_2 is always greater than the equilibrium $CaCO_3$ decomposition pressure for atmospheric pressure carbonation at 650 °C. From an operational point of view, it is also important to know the limestone weight fraction of the bed material, shown by the dotted curve in Fig. 6.

A useful criterion to evaluate the gasification performance is the "cold gas efficiency", which indicates the proportion of the fuel heating value retained by the product gas [21]. As complete combustion of unreacted char (here in pure O_2) in the combustor is usually insufficient to provide all the heat required by the process, external heat (Q_{in}, kJ/h) is also supplied to the combustor. Consistent with Hofbauer et al. [23], we define the cold gas efficiency as

$$\eta_{CGE} = \frac{F_{P_2} \cdot \mathrm{LHV_{PG}} - Q_{in}}{m_{fuel} \cdot \mathrm{LHV_{fuel}}} \tag{24}$$

where F_{P2} and $\mathrm{LHV_{PG}}$ (kJ/kmol) are the molar flow rate and lower heating value of the dry product gas generated by the gasifier, and m_{fuel} and $\mathrm{LHV_{fuel}}$ (kJ/kg) are for dry and ash-free biomass, respectively. Another way to compare the results with and without lime [3] is to define the overall process efficiency as the ratio of the energy output from the H_2 produced, discounting the heat necessary to drive the reaction process (Q_{in}), to the energy input from the biomass

$$\eta_{H2} = \frac{m_{H2} \cdot \mathrm{LHV}_{H2} - Q_{in}}{m_{fuel} \cdot \mathrm{LHV_{fuel}}} \tag{25}$$

Fig. 7 compares the cold gas efficiency, H_2 production efficiency, total solid circulation rate of bed material, and mean solids residence time within the gasifier of the non-enhanced (solid curves) and lime-enhanced (dashed curves) processes. While for non-enhanced biomass gasification, 100% inert silica sand (SiO_2) is used as the bed material, for lime-enhanced biomass gasification, different weight fractions of limestone are obtained from energy balance calculations. Increasing the moisture content of the fuel leads to decreased cold gas efficiencies, mostly due to additional heating required for moisture evaporation in the gasifier and endothermic steam gasification of biomass promoted by increasing the system H_2O concentration. At constant temperatures of both beds, the additional external heating requirement of the gasifier is met by increasing the sensible heat provided by higher circulation of bed material from the higher-temperature combustor to the gasifier. Therefore, at a constant CaO/Fuel mass ratio (=8) and constant total gasifier solids inventory, more sand circulates from the combustor to the gasifier, leading to lower solids residence time and less limestone within the gasifier (dotted curve). For equal carbon conversion and given temperatures of the two beds, the cold gas efficiency of lime-enhanced steam gasification (dashed curves) is less than for non-enhanced gasification because of the additional external heating requirements for sorbent calcination within the regenerator. For lime-enhanced gasification, due to the *in situ* heat generated by the exothermic carbonation reaction within the gasifier, the dependence on the sensible heat carried by solids passing between the two beds is reduced, and the total solids circulation ratio, (CaO + Sand)/Fuel, is predicted to be considerably lower. Finally, lime-enhanced biomass gasification is predicted to have slightly better performance in terms of the H_2 production efficiency. Therefore, using limestone in fluidized bed gasifiers for high-temperature CO_2 capture is particularly interesting if the production of a H_2-rich product gas is a major objective. It should also be noted that in this study, consistent with the literature [47], the comparison of non-enhanced and lime-enhanced biomass gasification is based on the moisture content of the fuel. However, the additional temperature and pressure constraints that simultaneous carbonation and calcination of limestone impose on the gasifier and combustor beds make the comparison more difficult. For instance, while higher gasifier bed temperatures (700–850 °C) are usually desirable for effective tar cracking, a lower operating temperature window (650–700 °C) must be observed for effective CO_2 capture at atmospheric pressure.

5. Conclusions

A relatively simple model is developed to capture the essence of integrated biomass gasification with cyclic CO_2 capture in a dual fluidized bed reactor, with limestone particles constituting, all or a fraction of, the bed material. Conversion of solid biomass particles to dominant gaseous products (H_2, CO, CH_4 and CO_2) is modeled by a simple stoichiometric equilibrium model. By adopting an empirical kinetic model for the carbonation rate of limestone particles from the literature, not only is the effect of sorbent loss of reactivity due to sintering during cyclic operation taken into account, but the dependencies of the average carbonation conversion of CaO particles on operating parameters such as carbonation temperature, CO_2 partial pressure and mean residence time of sorbent particles within the carbonator are also clarified. There is considerable scope for refining the model in future work, for example to allow for the effect of sorbent attrition and the energy required for air separation. However, the model provides a basic tool to describe the general trends of the process and to identify the effects of key operating variables. Moreover, the model is useful in the identifying promising process design and operating conditions.

Acknowledgement

The authors acknowledge Charles Allan from Loughborough University (UK) who contributed to the initiation of this research for his perseverance in his undergraduate project.

References

[1] Corella J, Toledo JM, Molina G. A review on dual fluidized-bed biomass gasifiers. Ind Eng Chem Res 2007;46:6831–9.
[2] Corella J, Toledo JM, Molina G. Biomass gasification with pure steam in fluidised bed: 12 variables that affect the effectiveness of the biomass gasifier. Int J Oil Gas Coal Technol 2008;1:194–207.
[3] Florin NH, Harris AT. Enhanced hydrogen production from biomass with in situ carbon dioxide capture using calcium oxide sorbents. Chem Eng Sci 2008;63:287–316.
[4] Curran GP, Fink CE, Gorin E. CO_2 acceptor gasification process – studies of acceptor properties. Adv Chem Ser 1967;69:141–65.
[5] Hanaoka T, Yoshida T, Fujimoto S, Kamei K, Harada M, Suzuki Y, et al. Hydrogen production from woody biomass by steam gasification using a CO_2 sorbent. Biomass Bioenergy 2005;28:63–8.
[6] Pfeifer C, Puchner B, Hofbauer H. In-situ CO_2-absorption in a dual fluidised bed biomass steam gasifier to produce a hydrogen rich syngas. Int J Chem Reactor Eng 2007;5:A9.
[7] Pfeifer C, Puchner B, Pröll T, Hofbauer H. H2-rich syngas from renewable sources by dual fluidized bed steam gasification of solid biomass. In: ECI Conference. the 12th international conference on fluidization. Vancouver, Canada: New Horizons in Fluidization Engineering; 2007.
[8] Lv PM, Xiong ZH, Chang J, Wu CZ, Chen Y, Zhu JX. An experimental study on biomass air–steam gasification in a fluidized bed. Bioresour Technol 2004;95:95–101.
[9] Corella J, Toledo JM, Molina G. Steam gasification of coal at low-medium (600–8000 °C) temperature with simultaneous CO_2 capture in fluidized bed at atmospheric pressure: the effect of inorganic species. 1. Literature review and comments. Ind Eng Chem Res 2006;45:6137–46.
[10] Ammendola P, Chirone R, Miccio F, Ruoppolo G, Scala F. Devolatilization and attrition behavior of fuel pellets during fluidized-bed gasification. Energy Fuels 2011;25:1260–6.
[11] Pfeifer C, Rauch R, Hofbauer H. In-bed catalytic tar reduction in a dual fluidized bed biomass steam gasifier. Ind Eng Chem Res 2004;43:1634–40.
[12] Devi L, Ptasinski KJ, Janssen FJJG. Review of the primary measures for tar elimination in biomass gasification processes. Biomass Bioenergy 2003;24:125–40.
[13] Corella J, Toledo JM, Molina G. Calculation of the conditions to get less than 2 g tar/Nm^3 in a fluidized bed biomass gasifier. Fuel Process Technol 2006;87:841–6.
[14] IPCC special report on carbon dioxide capture and storage. Cambridge, United Kingdom and New York, NY, USA: Cambridge University Press. 442pp.
[15] Sakadjian BB, Iyer MV, Gupta H, Fan LS. Kinetics and structural characterization of calcium-based sorbents calcined under subatmospheric conditions for the high-temperature CO_2 capture process. Ind Eng Chem Res 2007;46:35–42.
[16] Lu DY, Hughes RW, Anthony EJ, Manovic V. Sintering and reactivity of $CaCO_3$-based sorbents for in situ CO_2 capture in fluidized beds under realistic calcination conditions. J Environ Eng 2009;135:404–10.
[17] Hughes RW, Lu DY, Anthony EJ, Macchi A. Design, process simulation and construction of an atmospheric dual fluidized bed combustion system for in situ CO_2 capture using high-temperature sorbents. Fuel Process Technol 2005;86:1523–31.
[18] Donat F, Florin NH, Anthony EJ, Fenell PS. The influence of high-temperature steam on the reactivity of CaO sorbent for CO_2 capture. Environ Sci Technol 2012;46:1262–9.
[19] Kaushal P, Pröll T, Hofbauer H. Model for biomass char combustion in the riser of a dual fluidized bed gasification unit: Part 1 – model development and sensitivity analysis. Fuel Process Technol 2008;89:651–9.
[20] Kunni D, Levenspiel O. Fluidization engineering. 2nd ed. Boston, MA: Butterworth-Heinmann; 1991.
[21] Li XT, Grace JR, Lim CJ, Watkinson AP, Chen HP, Kim JR. Biomass gasification in a circulating fluidized bed. Biomass Bioenergy 2004;26:171–93.
[22] Watkinson AP, Lucas JP, Lim CJ. A prediction of performance of commercial coal gasifiers. Fuel 1991;70:519–27.
[23] Schuster G, Loffler G, Weigl K, Hofbauer H. Biomass steam gasification – an extensive parametric modelling study. Bioresour Technol 2001;77:71–9.
[24] Li XT. Biomass gasification in a circulating fluidized bed. PhD thesis. Department of Chemical and Biological Engineering, University of British Columbia; 2002.
[25] Pröll T, Hofbauer H. Development and application of a simulation tool for biomass gasification based processes. Int J Chem Reactor Eng 2008;6:A89.
[26] McBride BJ, Gordon S, Reno MA. Coefficients for calculating thermodynamic and transport properties of individual species. NASA Technical Memorandum 4513, NASA; 1993.
[27] Merrick D. Mathematical models of the thermal decomposition of coal– Parts 1–6. Fuel 1988;62:534–70.
[28] Dooley B. Release on the IAPWS industrial formulation 1997 for the thermodynamic properties of water and steam. Palo Alto CA: IAPWS Secretariat, EPRI; 1997.
[29] Burcat A, McBride B. Ideal gas thermodynamic data for combustion and air pollution use. Report No. TAE 804. Technion Israel Institute of Technology, Aerospace Engineering; 1997.
[30] Lin S, Harada M, Suzuki Y, Hatano H. Continuous experiment regarding hydrogen production by coal/CaO reaction with steam (II) solid formation. Fuel 2006;85:1143–50.
[31] Sun P, Grace JR, Lim CJ, Anthony EJ. The effect of CaO sintering on cyclic CO_2 capture in energy systems. AIChE J 2007;53:2432–42.
[32] Symonds RT, Lu DY, Hughes RW, Anthony EJ, Macchi A. CO_2 capture from simulated syngas via cyclic carbonation/calcination for a naturally occurring limestone: pilot-plant testing. Ind Eng Chem Res 2009;48:8431–40.
[33] Sun P, Lim CJ, Grace JR. Cyclic CO_2 capture by limestone-derived sorbent during prolonged calcination/carbonation cycling. AIChE J 2008;54:1668–77.
[34] Grasa GS, Abanades JC. CO_2 capture capacity of CaO in long series of carbonation/calcination cycles. Ind Eng Chem Res 2006;45:8846–51.
[35] Abanades JC, Alvarez D. Conversion limits in the reaction of CO_2 with lime. Energy Fuels 2003;17:308–15.
[36] Grasa GS, Alonso M, Abanades JC. Sulfation of CaO particles in a carbonation/calcination loop to capture CO_2. Ind Eng Chem Res 2008;47:1630–5.
[37] Ariasa B, Abanades JC, Grasa GS. An analysis of the effect of carbonation conditions on CaO deactivation curves. Chem Eng J 2011;167:255–61.

[38] Abanades JC. The maximum capture efficiency of CO_2 using a carbonation/calcination cycle of $CaO/CaCO_3$. Chem Eng J 2002;90:303–6.

[39] Rodriguez N, Alonso M, Abanades JC. Average activity of CaO particles in a calcium looping system. Chem Eng J 2010;156:388–94.

[40] Grasa GS, Abanades JC, Anthony EJ. Effect of partial carbonation on the cyclic CaO carbonation reaction. Ind Eng Chem Res 2009;48:9090–6.

[41] Johnsen K, Grace JR, Elnashaie SSEH, Eriksen D. Modeling of sorption-enhanced steam reforming in a dual fluidized bubbling bed reactor. Ind Eng Chem Res 2006;45:4133–44.

[42] Grasa GS, Abanades JC, Alonso M, Gonzales B. Reactivity of highly cycled particles of CaO in a carbonation/calcination loop. Chem Eng J 2008;137:561–7.

[43] Baker EH. The calcium oxide-carbon dioxide system in the pressure range 1–300 atm. J Chem Soc 1962:464–70.

[44] Alvarez D, Abanades JC. Determination of the critical product layer thickness in the reaction of CaO with CO_2. Ind Eng Chem Res 2005;44:5608–15.

[45] Romano MC. Modelling the carbonator of a Ca-looping process for CO_2 capture from power plant flue gas. Chem Eng Sci 2012;69:257–69.

[46] Weimer T, Berger R, Hawthorne C, Abanades JC. Lime enhanced gasification of solid fuels: Examination of a process for simultaneous hydrogen production and CO_2 capture. Fuel 2008;87:1678–86.

[47] Pröll T, Hofbauer H. H_2 rich syngas by selective CO_2 removal from biomass gasification in a dual fluidized bed system—process modelling approach. Fuel Process Technol 2008;89:1207–17.